ACS MATERIALS Au
AN OPEN ACCESS JOURNAL OF THE AMERICAN CHEMICAL SOCIETY

pubs.acs.org/materialsau
Article

Phase Chemistry for Hydration Sensitive (De)intercalation of Lithium Aluminum Layered Double Hydroxide Chlorides

Dongdong Li,*[,‖] Ning Zhang,[‖] Dandan Gao, Ziyu Zhuang, and Dewen Zeng

Cite This: ACS Mater. Au 2024, 4, 45−54

Read Online

ACCESS | Metrics & More | Article Recommendations | Supporting Information

ABSTRACT: Lithium aluminum layered double hydroxide chlorides (LADH-Cl) have been widely used for lithium extraction from brine. Elevation of the performances of LADH-Cl sorbents urgently requires knowledge of the composition−structure−property relationship of LADH-Cl in lithium extraction applications, but these are still unclear. Herein, combining the phase equilibrium experiments, advanced solid characterization methods, and theoretical calculations, we constructed a cyclic work diagram of LADH-Cl for lithium capture from aqueous solution, where the reversible (de)hydration and (de)intercalation induced phase evolution of LADH-Cl dominates the apparent lithium "adsorption−desorption" behavior. It is found that the real active ingredient in LADH-Cl type lithium sorbents is a dihydrated LADH-Cl with an Al:Li molar ratio varying from 2 to 3. This reversible process indicates an ultimate reversible lithium (de)intercalation capacity of ∼10 mg of Li per g of LADH-Cl. Excessive lithium deintercalation results in the phase structure collapse of dihydrated LADH-Cl to form gibbsite. When interacting with a concentrated LiCl aqueous solution, gibbsite is easily converted into lithium saturated intercalated LADH-Cl phases. By further hydration with a diluted LiCl aqueous solution, this phase again converts to the active dihydrated LADH-Cl. In the whole cyclic progress, lithium ions thermodynamically favor staying in the Al−OH octahedral cavities, but the (de)intercalation of lithium has kinetic factors deriving from the variation of the Al−OH hydroxyl orientation. The present results provide fundamental knowledge for the rational design and application of LADH-Cl type lithium sorbents.

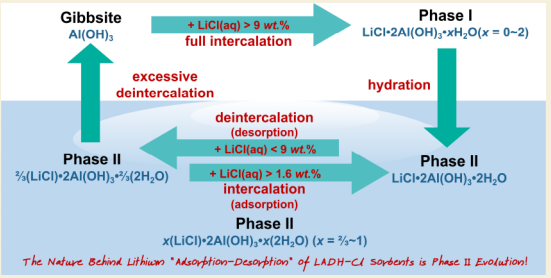

KEYWORDS: *lithium, sorbent, LADH-Cl, phase evolution, hydration, intercalation, deintercalation*

INTRODUCTION

Lithium aluminum layered double hydroxide chlorides (LADH-Cl) have been successfully used as industrial lithium sorbents, supporting a lithium carbonate productivity over decade thousand tons.[1−5] Technology based on the LADH-Cl sorbents makes it possible to extract lithium from low grade brine resources, mitigating the lithium pressure at least in this century.[6] For decades, the interaction between LADH-Cl and aqueous lithium ion has been labeled as "adsorption−desorption". However, excessive desorption of lithium from LADH-Cl results in the decomposition of LADH-Cl and the formation of crystalline aluminum hydroxide, e.g., gibbsite or bayerite.[7,8] This indicates that phase evolution is very likely behind the apparent adsorption−desorption behavior. However, to date, the fundamental phase chemistry, especially phase composition, structure, evolution, thermodynamics, and transition kinetics, of the LADH-Cl is far from clear.

The chemical formula of LADH-Cl is usually written as mLiCl·2Al(OH)$_3$·nH$_2$O, in which the stoichiometric factors m and n have not been constrained.[2,9−11] Anhydrous phase LiCl·2Al(OH)$_3$ and hydrated phases LiCl·2Al(OH)$_3$·H$_2$O, LiCl·2Al(OH)$_3$·1.5H$_2$O, and LiCl·2Al(OH)$_3$·2H$_2$O have been reported as stoichiometric compounds. Their structures have been determined from powder or single crystal diffraction and solid-state magic-angle-spinning NMR (ssNMR) technics.[12−16] More extensively, the nonstoichiometric nature of LADH-Cl has been invoked. First, the hydration number in LADH-Cl is volatile. Even though it is usually reported as an integer, it is actually an approximation of the experimental determination.[16] In most cases, the determined hydration number is far from the integer, and varies from ∼0 to 3.5.[2,7,9,10,16−19] Up until now, when LADH-Cl is used as a lithium sorbent, if the hydration number of LADH-Cl will change, how it changes and to what extent it can change are still blind spots. Second, the Al:Li molar ratio in LADH-Cl is also volatile and varies from ∼2 to 3.5. To avoid the question of the real composition of LADH-Cl sorbent, some researchers even described their samples using nominal Al:Li, that is, the whole Al:Li of the raw materials.[18] However, this makes our understanding of active

Received: July 31, 2023
Revised: September 22, 2023
Accepted: September 22, 2023
Published: October 6, 2023

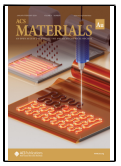

ingredients in the so-called LADH-Cl sorbent more confusing. Besides, in usual adsorption−desorption studies, only the concentration of lithium in aqueous solution is of interest, while the composition and structure variations of the sorbent are overlooked, unless the sorbent is destroyed or loses its function.

LADH-Cl is synthesized from and used in an aqueous environment. Mother liquid adhesion makes it very difficult to determine the composition of the "pure solid LADH-Cl".[9,10] Washing and drying procedures are useful for removing most adhesions and have been widely adopted in careful composition and structure investigations of LADH-Cl.[12,14,16,17,20,21] However, the washing procedure can easily change the LiCl and water contents, and even the structure of LADH-Cl.[22] Morever, the water content of LADH-Cl is very sensitive to the drying conditions, e.g., temperature, humidity, and time.[23] Consequently, the determined composition of the "cleaned" LADH-Cl sample is likely different from the raw one that equilibrated with its mother liquid. As a result, the composition, structure, and evolution of LADH-Cl in lithium extraction application are still unknown. This knowledge gap has become the biggest obstacle for the rational design and application of LADH-Cl type lithium sorbents.

Herein, we experimentally determined phase diagrams of the $Al(OH)_3$-LiCl-H_2O system at 348.15 K, using well structured gibbsite and gibbsite-derived LADH-Cl as initial reactants, respectively. The composition and structure of LADH-Cl are closely related to the concentration of LiCl aqueous solution, and all of the produced LADH-Cl is hydrated. Whether we used gibbsite or gibbsite-derived LADH-Cl as the initial material, lithium saturated LADH-Cl with $n(Al):n(Li) = 2$, in which all the Al−OH octahedral cavities are filled with lithium (Phase I), formed in LiCl aqueous solution with concentrations higher than 9 wt %. The hydration number of Phase I was found to increase from ∼0.25 to 2, when the LiCl concentration varied from nearly saturated to about 9 wt %. Dihydrated LADH-Cl deintercalated LiCl when it interacted with pure water or dilute LiCl aqueous solution with concentration lower than 9 wt %, resulting in a lithium unsaturated LADH-Cl phase (Phase II). This suggests that the real active ingredient in LADH-Cl type lithium sorbents is Phase II. Other phases play their roles by first hydrating to dihydrate. Moreover, our results confirmed that the ultimate Al:Li molar ratio that preserves the crystal structure of Phase II is 3. Further deintercalation of LiCl from the ultimate Al:Li Phase II resulted in structure collapse and the formation of gibbsite. Our experiments also suggested that the full production of lithium unsaturated from gibbsite and dilute LiCl aqueous solution is hard, despite the thermodynamic support. Altogether, this evidence unambiguously suggested that the interaction between LADH-Cl sorbent and aqueous lithium is controlled by phase evolution, which results from the synergistic lithium-chloride-water deintercalation and intercalation. Powder X-ray diffraction (PXRD), ssNMR, Fourier transform infrared (FTIR), and Raman characterizations of the LADH-Cl samples gave refined structure variation of the two types of hydrated LADH-Cl phases. Thermodynamically, ab initio molecular dynamics (AIMD) and density functional theory (DFT) simulations showed that lithium atoms located in the Al−OH octahedral cavities of LADH-Cl are more stable than those located in the interlayer.

METHODS

Experimental Section

The raw materials used in this study are gibbsite (γ-$Al(OH)_3$, CAS: 21645-51-2, Shanghai Macklin Biochemical Co., Ltd., <20 μm, 99.8%), synthesized LADH-Cl Raw1 and Raw2, anhydrous lithium chloride (CAS: 7447-41-8, Shanghai Aladdin Biochemical Technology Co., Ltd., 98%), and ultrapure water (UPT-II-20T, Chengdu Ultrapure Technology Co., Ltd., 18.2 MΩ·cm). Detailed preparation and characterization of these raw materials are summarized in Supplementary Section 1.

An isothermal method was used to determine the solid−liquid phase equilibria in the ternary system $Al(OH)_3$-LiCl-H_2O. The experiments were conducted at 348.15 K. A Lauda Command thermostatic water bath was used to create a constant temperature environment. Temperature uncertainty of the whole thermostat system was controlled within 0.05 K. Penicillin bottles (20 mL) with a butyl rubber stopper and aluminum cap were used as sample containers. The reaction mixtures were prepared by weighing gibbsite or Raw1 (∼3 g) and an appropriate amount of lithium chloride aqueous solution of various concentrations (∼9 mL). Magnetons coated with PTFE were also placed into these bottles. Then, these bottles with samples and magnetons were placed into a multichannel magnetic stirrer with a speed of ∼300 rpm. The detailed procedure and setup are summarized in Supplementary Section 2.

All solid samples were characterized by PXRD (Bruker D8 Advance diffractometer, Cu Kα radiation, λ_1 = 1.5406 and λ_2 = 1.5444, ratio $K\alpha_2/K\alpha_1$ = 0.5) operated in reflection geometry. Data were collected at a continuous scan rate of 38 s per step and a step size of 0.02° 2θ. For Rietveld refinement, data were recorded over 5−120° 2θ (step size of 0.01° 2θ, counting time 134 s per step). The structure determination of 0.25w LADH-Cl was carried out by Rietveld refinement using the FullProf program (Version September-2019).[24] For the refinement, a pseudo-Voigt line shape function with five variables was used to fit the experimental profile. The background was corrected using a 6-coefficient polynomial function. For solving the structure of 0.25w LADH-Cl, we used the structure of 0w LADH-Cl reported by Besserguenev et al.[12] as an initial trial model. To account for the disorder of the interlayered water molecules and chloride ions, we gave a hexagonal space group $P63/m$, which differs from that of the $P63/mcm$ space group of 0w LADH-Cl.

ssNMR spectra were collected at room temperature on a Bruker AVANCE NEO 400 WB spectrometer equipped with a 9.4 T magnet, using a Bruker 4 mm MAS triple-resonance probe. All samples were loaded into 4 mm zirconia rotors and spun at 12 kHz. For ^{7}Li ssNMR experiments a typical 30° pulse and recycle delay time of 5 s were used. The ^{7}Li chemical shift was externally referenced to a 1 M LiCl solution and a secondary reference anhydrous LiCl. For ^{27}Al ssNMR experiments, the recycling delay was 2 s. The ^{27}Al chemical shift was externally referenced to that of solid Al_2O_3. The ^{7}Li spectrum resonates at 155.52 MHz. The ^{27}Al resonates at 104.27 MHz. All fits to the ssNMR spectra were made using the program DMFIT.[25]

FTIR spectra of the solid samples studied in this study were obtained by using a Nexus ThermoNicolet Spectrometer equipped with a DTGS KBr detector. All of the samples were dried at ambient conditions for several days. The FTIR measurement was performed at room temperature. The spectra were collected with 32 scanning times and a resolution of 4 cm^{-1} over the spectral range between 400 and 4000 cm^{-1}. Raman spectra were obtained on a laser-confocal microspectrometer (Thermo Scientific DXR2). The laser wavelength used is 532 nm. Raman shifts were observed in the spectral range from 50 to 4000 cm^{-1} with a resolution of 4 cm^{-1}. All fits to the Raman spectra were made using the program DMFIT.[25]

The scanning electron microscopy (SEM) studies were performed on a JSM-5610LV/INCA scanning electron microscope (Oxford Instruments, Abingdon, Oxfordshire, UK). The excitation voltage used was 2 kV. The transmission electron microscopy (TEM) and selected area electron diffraction (SAED) experiments were carried out on a JEM-F200 transmission electron microscope at an acceleration voltage of 200 kV.

https://doi.org/10.1021/acsmaterialsau.3c00063
ACS Mater. Au 2024, 4, 45−54

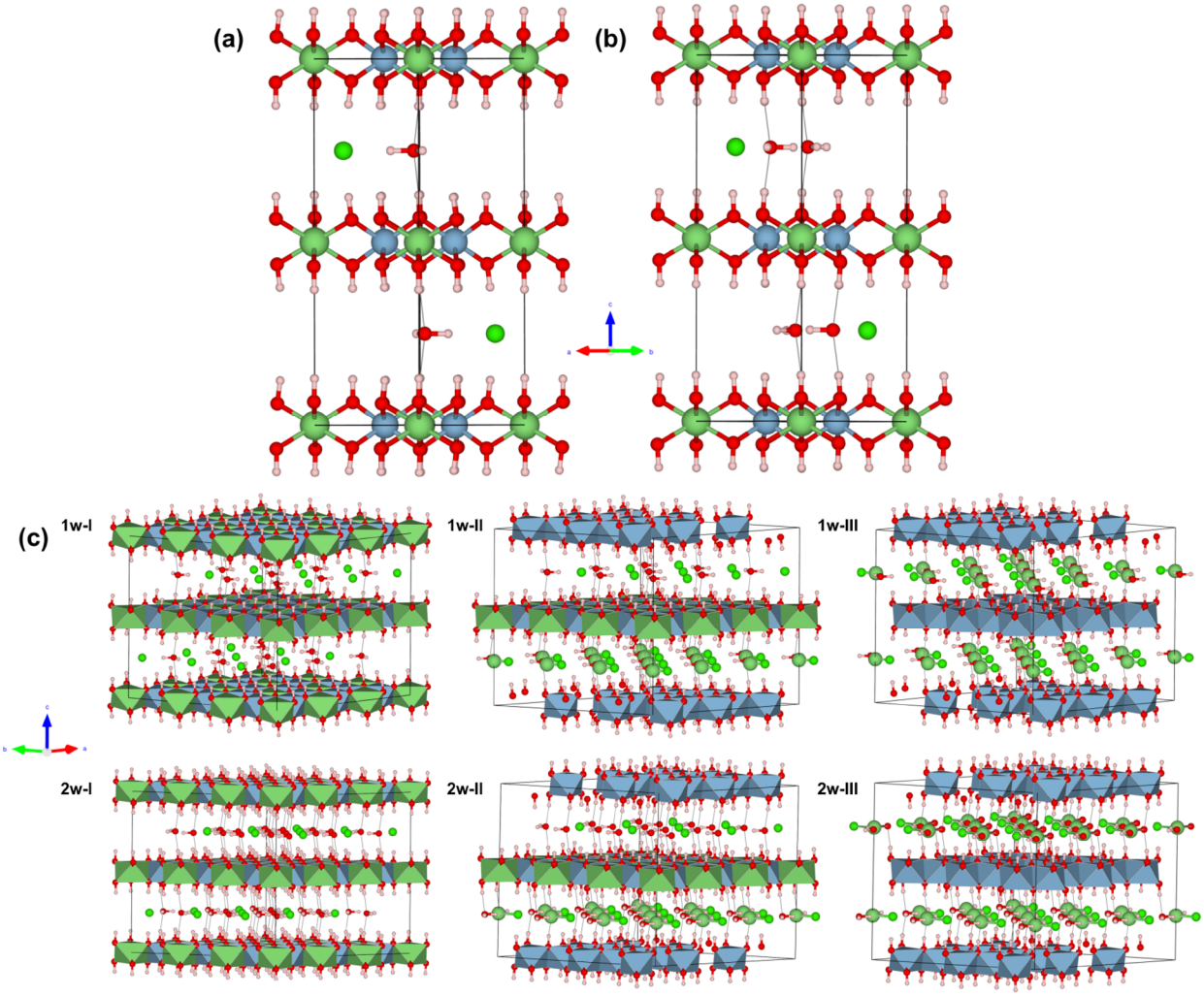

Figure 1. DFT optimized unit cells and the initial AIMD guesses of 1w and 2w LADH-Cl. (a) DFT optimized unit cell of 1w LADH-Cl. (b) DFT optimized unit cell of 2w LADH-Cl. (c) Initial AIMD guesses of "structured Li configuration" (I) and "unstructured Li configuration" (II and III). Large green balls: Li atoms. Large blue balls: Al atoms. Small green balls: Cl atoms. Red balls: O atoms. White balls: H atoms.

Theoretical Section

Initial structures for 1w and 2w LADH-Cl were constructed based on the reported 0w LADH-Cl,[12] by reducing the symmetry to *P*1 and adding stoichiometric water molecules. All of the added water molecules in the initial guesses are fully ordered. These initial guesses were further optimized by DFT calculations. These DFT optimized structures of interlayer disorder 1w and 2w LADH-Cl (Figure 1a and b) were then used for AIMD simulations at 300 K.

In all the AIMD simulations, the positions of all Al atoms were fixed to avoid the twisting of layers. To generate the different initial configurations (focusing on the position of Li atoms), the constructed systems of "unstructured Li configuration LADH-Cl" were prerelaxed with an equilibration run for 5 ps in unconstrained, constrained *z* direction, and constrained*xyz* direction of all Li atoms models (Figure 1c). Finally, for each simulation, a production run was performed for 10 ps, after an equilibration run for at least 5 ps. In the these simulations, a time step of 0.5 fs and hexagonal boxes with a volume of 3191.24 and 3300.53 Å^3 for 1w and 2w LADH-Cl, respectively, using periodic boundary conditions to eliminate interface effects were employed. See Supplementary Section 7 for the parameter setup of the AIMD simulations.

To estimate the stability of these "unstructured and structured Li configuration LADH-Cl", we randomly extracted 5 structures from the last 2.5 ps dynamics trajectories of each simulation. The static energies of these structures were further calculated. It should be noted that the positions of the Li and Al atoms are fixed in the optimizations to keep their original states in dynamic simulations as much as possible.

RESULTS AND DISCUSSION

Phase Diagrams and Phase Evolution

Figure 2 shows the measured phase diagrams of the $Al(OH)_3$-LiCl-H_2O system at 348.15 K. Here, we selected a temperature of 348.15 K to study, because the reaction kinetics is too slow to reach equilibrium at low temperature in affordable time. Even at 348.15 K, we found that 90 days is still necessary to get equilibrium data. Moreover, this temperature setup consists of the usual LADH-Cl synthesis and application conditions in laboratory experiments and industrial plants, i.e., 313−363 K. The experimental data are summarized in Table S2. Two reaction paths, i.e., the synthesis of LADH-Cl from gibbsite and LiCl(aq) solution as raw materials (Figure 2a, Z series) and the decomposition of LADH-Cl under the environment of LiCl(aq) solution (Figure 2b, F series), were considered in our experiments. Because the complete elimination of mother liquid adhesion without any change on the solids is impossible, here we adopted the Schreinemakers wet residual method[26,27] to derive the solid composition from experimentally determined liquid and wet-solid compositions. The so-called

https://doi.org/10.1021/acsmaterialsau.3c00063
ACS Mater. Au 2024, 4, 45−54

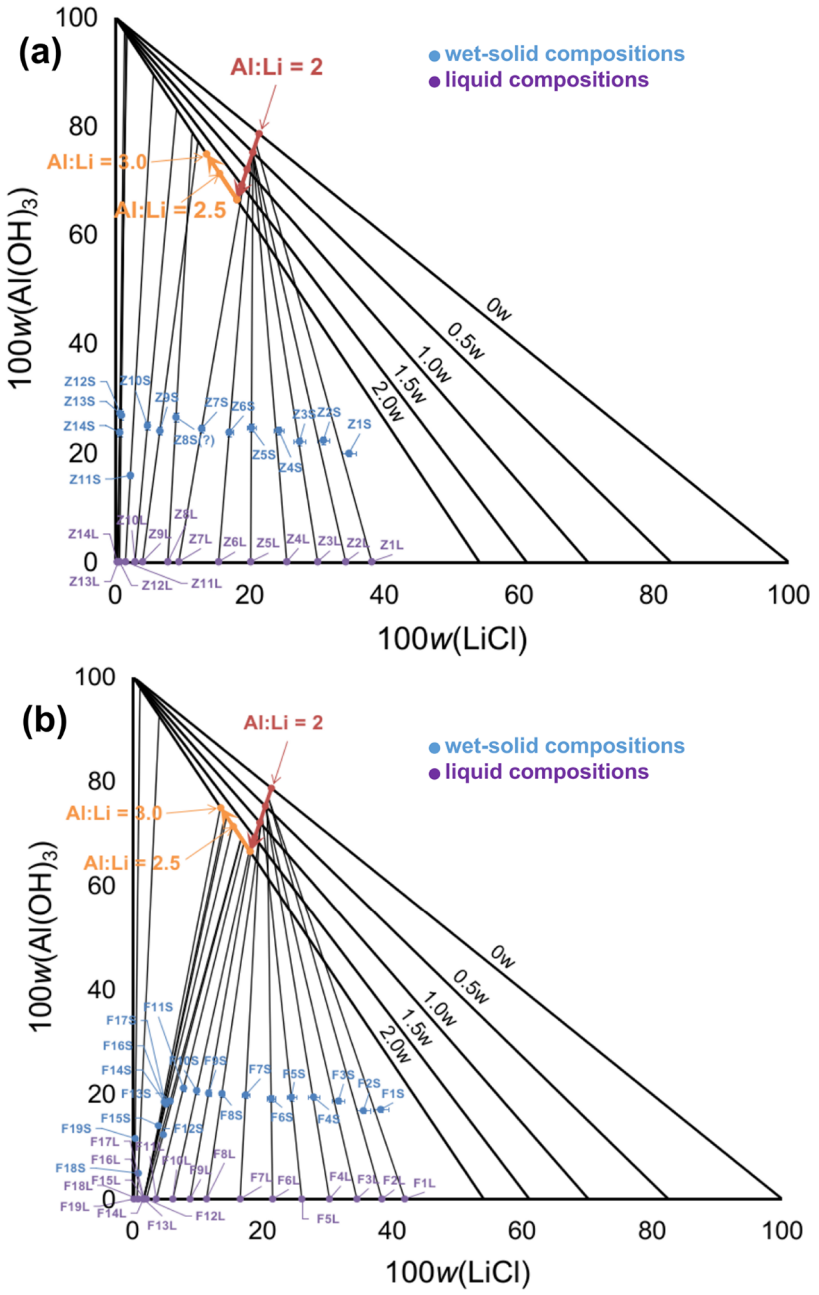

Figure 2. Phase diagrams of the $Al(OH)_3$-LiCl-H_2O system determined at 348.15 K for 90 days equilibration time. (a) Gibbsite and LiCl(aq) solution were used as initial materials (Z series). (b) Synthesized LADH-Cl Raw1 and LiCl(aq) solution were used as initial materials (F series). Thin black lines: tie lines consisting of liquid and wet-solid. Dark red arrow line: composition evolution line of Phase I. Yellow arrow line: composition evolution line of Phase II.

"wet-solid" is a mixture of coexisting solid and liquid. The intersection point of the "wet-solid"−liquid tie line (thin black lines in Figure 2) and solid composition line (thick red and orange lines with arrow in Figure 2) are the determined solid composition. Moreover, PXRD was used for detecting the phase transition and evolution of the solids separated from the equilibrium experiments. Wet solids were processed with filter paper to remove most of the entrainment, and we obtained powder samples suitable for PXRD analysis. The PXRD patterns of these powder samples were collected as quickly as possible, in the case of further change resulting from (de)hydration. The PXRD results are shown in Figure 3. Due to the negligible diffraction signal of the adhered mother liquid, the collected PXRD pattern can be attributed to the solid part.

The solid compositions and PXRD patterns suggested two types of LADH-Cl in the $Al(OH)_3$-LiCl-H_2O reaction system at 348.15 K. One is lithium saturated LADH-Cl with $n(Al):n(Li) = 2$ (Phase I). Another is lithium unsaturated LADH-Cl with $n(Al):n(Li)$ varied from 2 to 3 (Phase II). It is noticeable that all the LADH-Cl types are hydrated, while the hydration number is varied. Besides, our experiments suggested unreported lithium saturated LADH-Cl with a hydration number close to zero (samples Z1S, F1S, and F2S). Even the PXRD patterns of these samples are well reproducible, but they are significantly different from the

https://doi.org/10.1021/acsmaterialsau.3c00063
ACS Mater. Au 2024, 4, 45−54

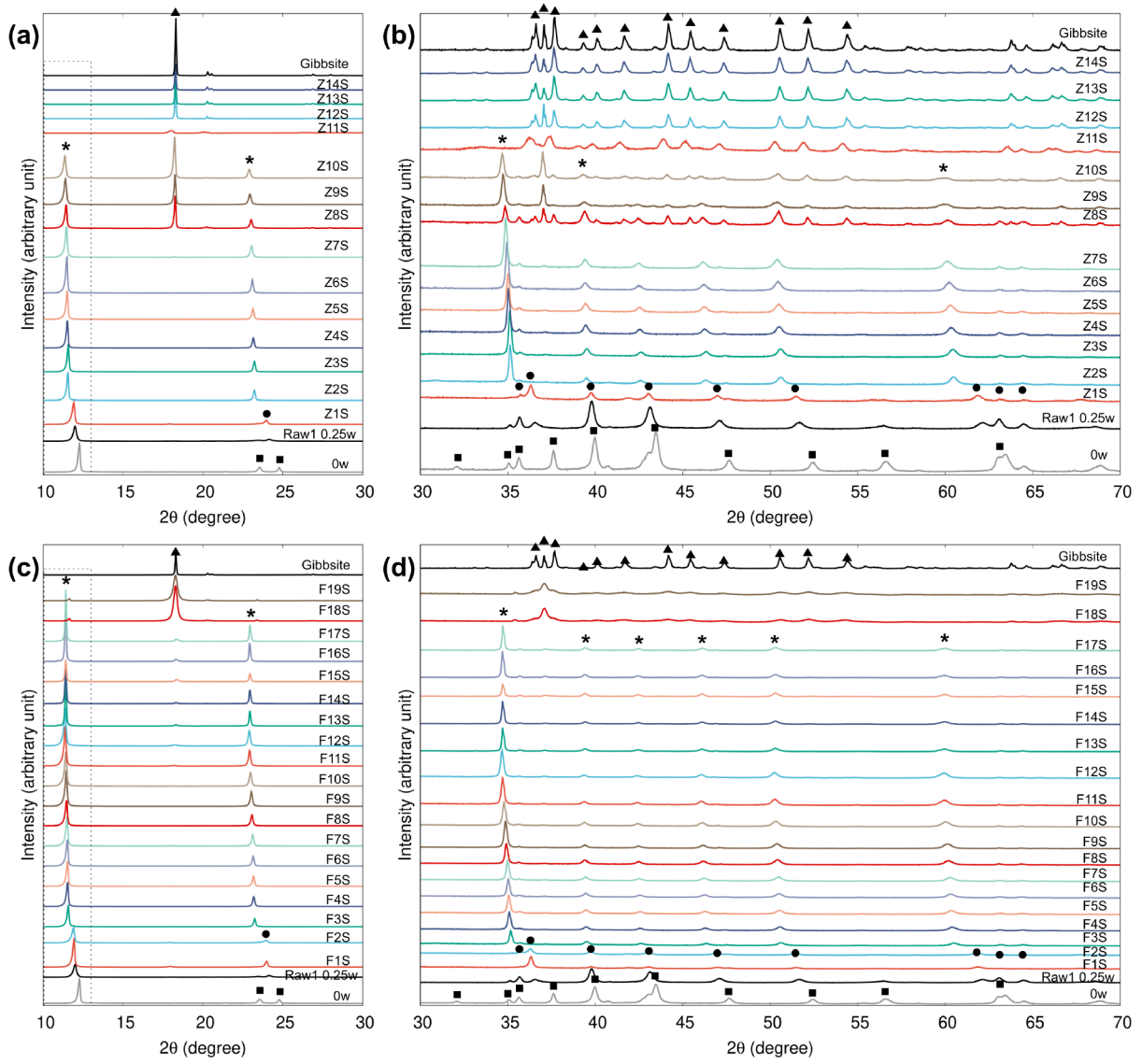

Figure 3. PXRD patterns of the solid samples separated from the phase diagram experiments. (a, b) Z series samples. (c, d) F series samples. * indicates the peaks of Phase I and II with hydration number from 0.5 to 2.0, ▲ indicates the peaks of gibbsite, ● indicates the peaks of 0.25w LADH-Cl, and ■ indicates the peaks of 0w LADH-Cl.

widely reported anhydrous, 1w, 1.5w, and 2w phases (Figure S14). The uncertainty for the hydration number derived from the wet residual analysis is about 0.3, which likely exceeded the hydration number of the new phase. Therefore, its hydration state cannot be well constrained from merely the wet residual analysis. Nevertheless, the hydration number can still be restrained to 0−0.5. Interestingly, we found that the PXRD patterns of these unreported lithium saturated LADH-Cl are the same as those of the synthesized Raw1 and Raw2 LADH-Cl (Figures S6 and S8). TG-DSC analysis of Raw1 and Raw2 (Figures S5 and S7) and chemical analysis of Raw1 (Table S1) showed a hydration number of about 0.25 ± 0.05. Accordingly, we suggest the presence of likely 0.25w LADH-Cl in our phase diagrams. The crystal structure of 0.25w LADH-Cl (Raw1 and Raw2) was solved using Rietveld refinement, showing hexagonal symmetry with the *P*63/*m* space group (Table S3, Figures S11 and S12). Like all the reported LADH-Cl, Al and Li atoms are well ordered in the 0.25w LADH-Cl (CCDC 2271308 and 2271309). Half of the Cl atoms are ordered, and the Cl and Li atoms line up parallel to the *c*-axis and form an alternating Li−Cl−Li chain, which is similar to those in the anhydrous phase.[12] However, the other Cl atoms are dislocated in the z = 0.25 plane. Besides, an unreported 0.5w lithium saturated LADH-Cl was suggested by our phase diagrams. Its structure was also solved using Rietveld refinement and determined as a hexagonal crystal with a *P*63/*m* space group (CCDC 2271319). Unlike the 0w and 0.25w LADH-Cl, but like 1w, 1.5w, and 2w, all the Cl atoms in the 0.5w LADH-Cl are disordered. Even though the anhydrous phase has been widely reported in the literature, we assert that it is unstable in LiCl(aq) solution at 348.15 K. Eventually, PXRD analysis of the 0.25w phase under dry N_2 atmosphere shows the same patterns as the 0w phase (CCDC 2271025), even at ambient temperature (Figure S6). This suggests that the formation of the anhydrous phase needs extremely dry conditions created by a dry N_2 atmosphere as done here or a vacuum drybox as in the literature.[12]

From the phase diagrams (Figure 2), one can clearly see the phase evolutions. In concentrated LiCl(aq) solution, Phase I generates from gibbsite (Figure 2a) or preserves itself (Figure

https://doi.org/10.1021/acsmaterialsau.3c00063
ACS Mater. Au 2024, 4, 45−54

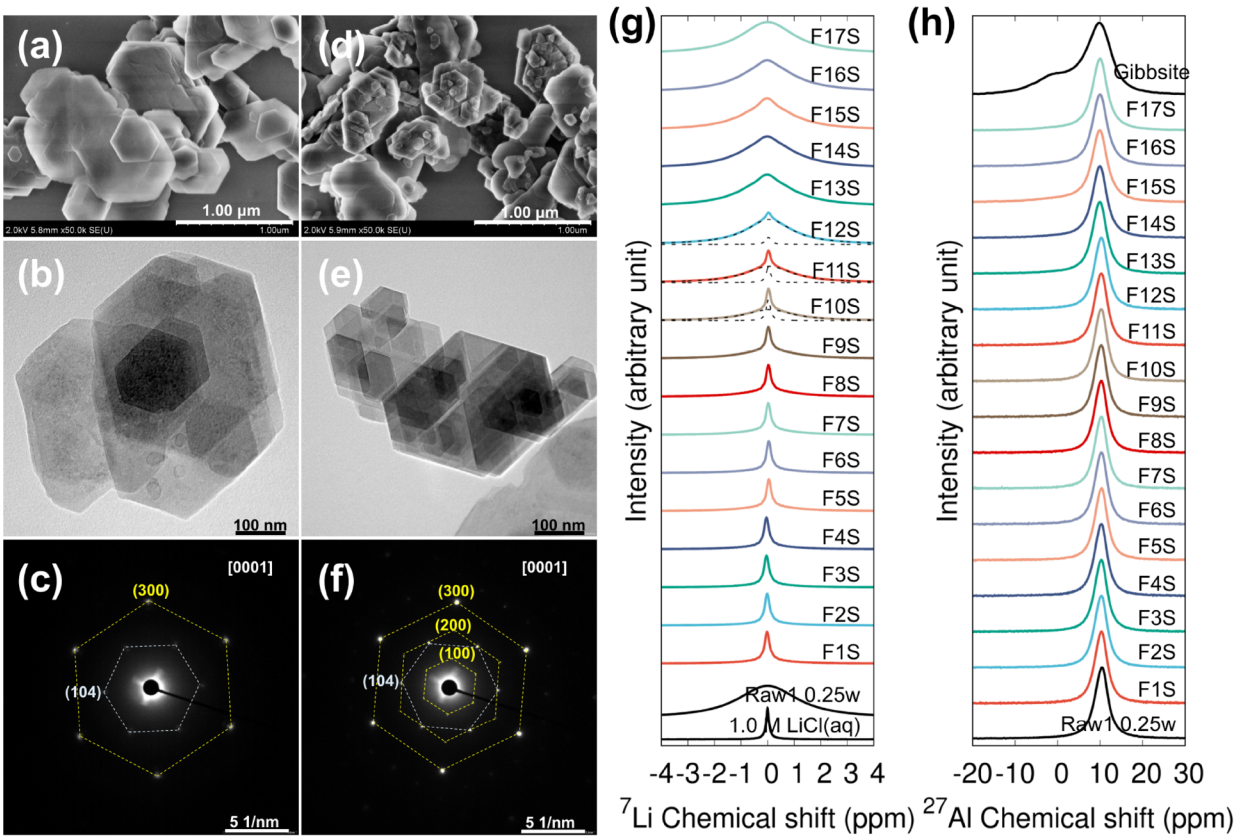

Figure 4. SEM, TEM, SAED, and ^{7}Li and ^{27}Al ssNMR characterizations of the F series samples. (a–c) SEM, TEM, and SAED images of sample F11S. (d–f) SEM, TEM and SAED images of sample F17S. (g,h) ^{7}Li and ^{27}Al ssNMR spectra of all F series samples.

2b). It changes from 0.25w to 2w, when the LiCl concentration varies from near saturation to about 9 wt %. Even with several scattered hydration states, i.e., 0.25w, 0.5w, 1w, 1.5w, and 2w, we suggest that the (de)hydration of Phase I from 0.25w to 2w is very likely continuous. This is because the symmetry of Phase I has not changed with the variation of hydration degree. When gibbsite reacted with dilute LiCl(aq) solution, i.e., <9 wt %, the conversions of gibbsite to LADH-Cl were weak, resulting in solid mixtures of gibbsite and Phase I (Figures 2a and 3a, Z8 to Z10) or pure gibbsite (Figures 2a and 3a, Z11 to Z14). Even though the apparent compositions of several mixtures (Figures 2a, Z8S and Z9S) were similar to Phase II (Figures 2b, F13S to F17S), the PXRD patterns undoubtedly showed the presence of unconverted gibbsite (Figure 3a, Z8S and Z9S). Usually, LADH-Cl is thought to form only when the LiCl(aq) solution concentration is higher than 4 mol/L, when using gibbsite as the initial material.[22,28] However, our experiments suggest a lower concentration limit, i.e., ∼0.7 mol/L (∼3 wt % as seen in Figure 2a, sample Z10L). The inconsistency likely results from the significantly different reaction time, indicating a very slow reaction kinetics between gibbsite and dilute LiCl(aq) solution. By contrast, Phase II instead of gibbsite formed when Phase I reacted with dilute LiCl(aq) solution, due to the deintercalation of LiCl. It is noticeable that the composition of Phase II is sensitive to the LiCl(aq) solution concentration. With the increase in concentration, LiCl intercalated into Phase II from aqueous solution. When lithium rich Phase II interacted with dilute LiCl(aq) solution, LiCl deintercalated from Phase II to an aqueous solution. Phase II is stable even in 0.38 mol/L LiCl(aq) solution (1.6 wt % as seen in Figure 2b, Z13L to Z17L), and its n(Al):n(Li) reversibly varied from 2 to 3. The LiCl (de)intercalation of Phase II shows apparent adsorption–desorption behavior and suggests a maximum reversible lithium adsorption–desorption capacity of ∼10 mg/g LADH-Cl. The predicted maximum capacity from the phase diagrams shows excellent consistency with available experiences,[7,8] suggesting the reasonability of the phase diagram for understanding the mechanism of LADH-Cl based lithium sorbents.

Sharp and strong PXRD peaks (Figure 3) indicate crystalline LADH-Cl, whether lithium is saturated or deintercalated. As for the solid samples separated from the phase diagram experiments, LADH-Cl crystals were observed from SEM images, showing similar sharpness and size as the initial gibbsites and 0.25w LADH-Cl (Figures 4a and d, and S2, S4, and S32–S37). The feature of intercalation products is widely presented, and the recrystallization phenomena is also evident. Small but regularly shaped LADH-Cl hexagonal sheet crystals were formed on the surface of large raw material particles as shown in the high magnification SEM (Figures 4a and d, and S34–S37) and TEM images (Figures 4b and e, and S38–S41). SAED images show clear single crystal diffraction spots of LADH-Cl (Figure 4c and f).

^{7}Li ssNMR spectra of these solid samples show a single peak at a chemical shift of ∼0 ppm (Figures 4g and S15–S19, refer to 1.0 M LiCl(aq) solution). However, all of these spectra can be divided into two components (Figures S15–S20, Table S5). One is a broad signal, and the second is a sharp signal. Both of them can be well represented with a Lorentzian line shape. Wimpenny et al.[22] have noticed the two reservoirs for lithium in some of their experimental samples. They attributed the

https://doi.org/10.1021/acsmaterialsau.3c00063
ACS Mater. Au 2024, 4, 45–54

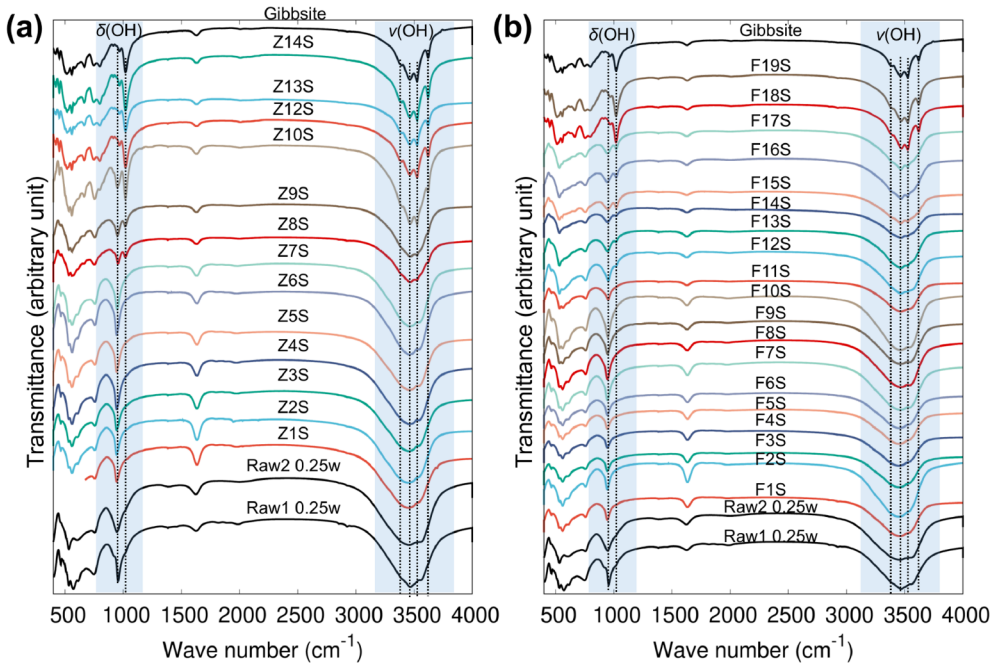

Figure 5. FTIR spectra of the solid samples separated from the phase diagram experiments. (a) Z series. (b) F series.

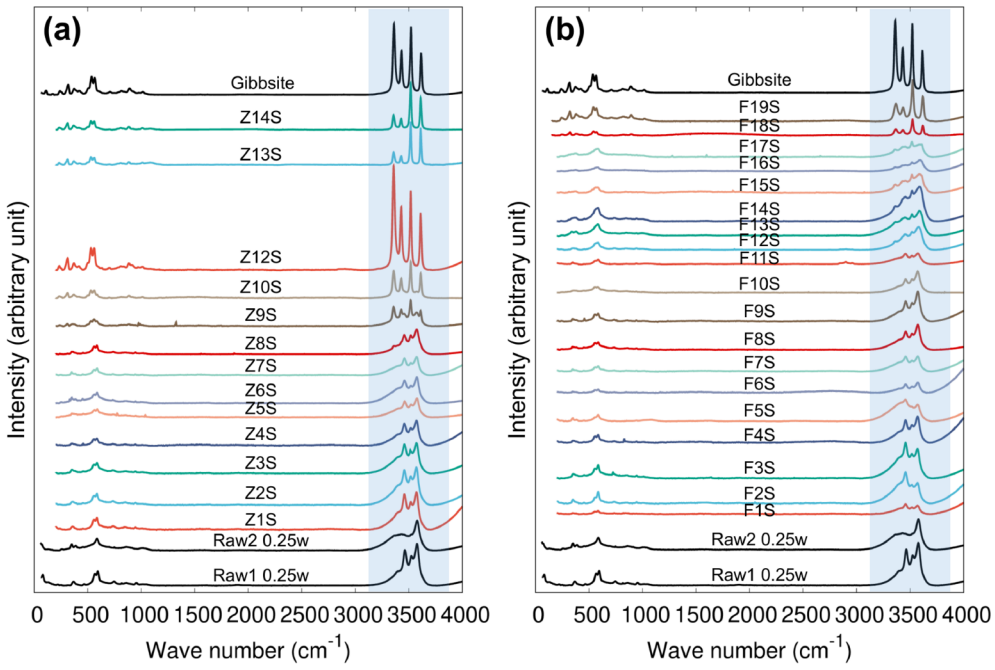

Figure 6. Raman spectra of the solid samples separated from the phase diagram experiments. (a) Z series. (b) F series.

sharp one to crystalline LADH-Cl and the broad one to a possible amorphous LADH-Cl. Herein, however, we attribute the sharp signal to an entrained LiCl(aq) solution instead of amorphous LADH-Cl, and the broad signal to crystalline LADH-Cl. In our results, the sharp ^{7}Li signal is centered over 0.01 ± 0.03 ppm with a width of 0.21 ± 0.02 ppm, which is consistent with the signal of the 1.0 M LiCl(aq) solution (centered over 0 ppm with 0.14 ppm width). The broad ^{7}Li signal is centered over 0.05 ± 0.03 ppm with a width of 2.04 ± 0.09 ppm, which is consistent with the signal of dried crystalline LADH-Cl (Raw1, 0.01 ppm with a width of 2.57 ppm). Deducting the effect of the ^{7}Li signal from LiCl(aq) adhesion, the ^{7}Li signals of these solid samples are all in good agreement. This indicates no ^{7}Li ssNMR detectable lithium coordination environment change with the variation of the hydration number and LiCl (de)intercalatation.

The ^{27}Al ssNMR results (Figure 4h, Table S6, and Figure S21) indicate that all the pure Phase I samples have only one signal (centered over ∼11.5 ppm with quadrupole coupling constant CQ = ∼1.5 MHz), which has nothing to do with the variation of the hydration number. For the mixed gibbsite and Phase I samples suggested by PXRD, the ^{27}Al spectra simultaneously show two quadrupole signals of gibbsite (one is centered over 10.75 ppm with CQ = ∼2.2 MHz, another is

https://doi.org/10.1021/acsmaterialsau.3c00063
ACS Mater. Au 2024, 4, 45−54

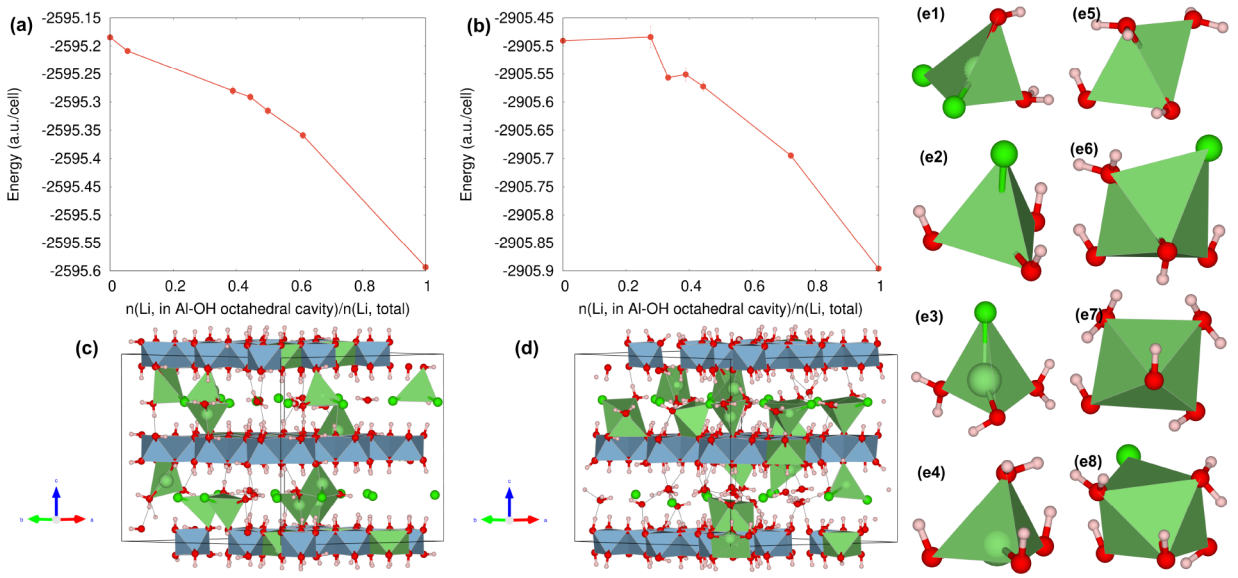

Figure 7. Theoretical simulation results of various 1w and 2w "structured Li configuration LADH-Cl" and "unstructured Li configuration LADH-Cl". (a) Static DFT energies of 1w LADH-Cl with various lithium atoms in Al−OH octahedral cavities. (b) Static DFT energies of 2w LADH-Cl with various lithium atoms in Al−OH octahedral cavities. (c, d) 1w and 2w frames after 15 ps, respectively. (e) Several typical local coordination structures of Li, (e1) to (e5) are tetrahedral, (e6) and (e7) are five-coordination, and (e8) is six-coordination. Large green balls: Li atoms. Large blue balls: Al atoms. Small green balls: Cl atoms. Red balls: O atoms. White balls: H atoms.

centered over 12.97 ppm with CQ = ∼4.2 MHz).[29] Due to the very low aluminum concentration (<0.0005 wt %) in the entrained mother liquid, we omit its contribution to the ^{27}Al spectra. Unlike Phase I samples, we found two ^{27}Al components in the spectra of Phase II samples F13S to F17S (Al:Li molar ratio = ∼3:1). One is consistent with that of Phase I (CQ = ∼1.5 MHz). Another is consistent with one signal of gibbsite (CQ = ∼4.2 MHz). These ^{27}Al ssNMR results indicate that Phase II is a new phase that differs from Phase I and gibbsite as suggested by PXRD. This also indicates that the lithium deintercalation from LADH-Cl can result in the variation of an Al−OH coordination environment.

FTIR and Raman spectra of the solid samples are shown in Figures 5 and 6. Pure Phase I samples showed similar FTIR and Raman spectra as the synthesized Raw1 and Raw2 LADH-Cl (Figures S24−S28 and Table S7), but different spectra to gibbiste (Figure S23). Moreover, the Raman spectra of Phase I and gibbsite in the ν(OH) region (3200 to 3800 cm^{-1}) are all consisted of four components.[30] The mixed samples Z8S, Z9S and Z10S showed instinct FTIR and Raman features of Phase I and gibbsite, which is consistent with PXRD and ssNMR analysis. The Raman spectra of pure Phase II samples, i.e., F11S to F17S, showed eight components (Figures S29−S31, Table S7), which is very different from those of Phase I, gibbsite, and their mixtures. Accordingly, these Raman spectra also suggested different hydroxyl stretching between Phase II and Phase I, even though they have nearly the same crystal stacking structure. In the short-range structure scale, the Raman results, together with ^{27}Al ssNMR, strongly indicated that the deintercalation of lithium in Phase II has resulted in extensive OH reorientation, which further promoted diverse hydrogen bonds and deformed Al−OH octahedrons.

AIMD and DFT Phase Stability Analysis

Extensive unbiased AIMD simulations were carried out to test the stability of various hydrated LADH-Cl configurations. Especially, we distinguished the "structured Li configuration LADH-Cl" and "unstructured Li configuration LADH-Cl". With respect to the "structured Li configuration LADH-Cl", we supposed that all the lithium atoms in LADH-Cl are located in the Al−OH octahedral cavities of the laminate. We supposed that some of the lithium atoms in LADH-Cl are located in the interlayer when the "unstructured Li configuration LADH-Cl" is mentioned. Due to the anhydrous LADH-Cl being well accepted as "structured Li configuration LADH-Cl" without a doubt, here we only studied hydrated LADH-Cl using 1w and 2w as examples.

The calculated static energies of these structures are shown in Figure 7a and b. The calculated average static energies for several systems indicate that the more structured Li is located in LADH-Cl the more stable it is, no matter for 1w or 2w LADH-Cl. Exactly, the formation energies should be used for comparing the thermodynamic phase stability. Here, however, the relation between phase stability and position of Li atoms is of interest for the same chemical formula. The relative phase stability of different formula, i.e. 1w and 2w LADH-Cl, was not discussed. As such, the reference static energy of the components that formed 1w and 2w LADH-Cl is the same all the time, respectively. Therefore, it is also reasonable to compare the thermodynamic phase stability using static energies. The simulations indicated that lithium atoms can not escape from the Al−OH octahedral cavities if they were placed there initially (Supplementary movies 1w-I-AIMD and 2w-I-AIMD). However, lithium atoms placed in the interlayer can spontaneously enter into the Al−OH octahedral lattice (Supplementary movies 1w-II-AIMD, 1w-III-AIMD, 2w-II-AIMD, and 2w-III-AIMD). These AIMD and DFT simulations enhance our conclusion drawn from experiments that all the lithium atoms in LADH-Cl are stable in the Al−OH octahedral lattice.

However, from these simulations, we noticed that not all interlayered lithium atoms spontaneously entered the Al−OH octahedral lattice in 15 ps. Figure 7c and d shows 1w and 2w frames after 15 ps. The number of lithium atoms that moved to

https://doi.org/10.1021/acsmaterialsau.3c00063
ACS Mater. Au 2024, 4, 45−54

the Al−OH octahedral lattice is highly dependent on the initial configuration after 5 ps prerelaxation. Therefore, in our affordable AIMD simulation time of ∼15 ps, we assert that all the AIMD simulations give metastable results. Nevertheless, these AIMD simulations evoke several noteworthy metastable local coordination structures of Li atoms. They are tetrahedral $Li(OH{-}Al)(Cl)_2(H_2O)$ (Figure 7e1), $Li(OH{-}Al)_3(Cl)$ (Figure 7e2), $Li(OH{-}Al)(Cl)(H_2O)_2$ (Figure 7e3), $Li(OH{-}Al)_3(H_2O)$ (Figure 7e4), and $Li(OH{-}Al)_2(H_2O)_2$ (Figure 7e5), five-coordination $Li(OH{-}Al)_3(H_2O)(Cl)$ (Figure 7e6) and $Li(OH{-}Al)_3(H_2O)_2$ (Figure 7e7), and six-coordination $Li(OH{-}Al)_3(H_2O)_2(Cl)$ (Figure 7e8). This suggests that the intercalation of lithium significantly involves the transition of tetrahedral to octahedral Li and the desolvation of Li from water and chloride coordinations. The AIMD simulations of "unstructured Li configuration LADH-Cl" also showed diverse hydrogen bonds and deformed Al−OH octahedrons as suggested from Raman and ^{27}Al ssNMR results. Li desolvation and the intralayer OH resulting from the deintercalation of Li are likely barriers that hinder the return of Li to the Al−OH octahedral cavity, resulting in a large active energy of apparent lithium "adsorption−desorption" behavior of the LADH-Cl sorbent.

CONCLUSION

In conclusion, the phase evolutions induced by reversible (de)hydration and (de)intercalation dominate the apparent lithium "adsorption−desorption" behavior of LADH-Cl. Crystalline LADH-Cl can bring the "adsorption−desorption" behavior out without the attribution of the amorphous phase. The phase diagrams of the $Al(OH)_3$-LiCl-H_2O system account for the physical chemistry mechanism of LADH-Cl sorbent well. The deintercalation of lithium together with chloride and water from lithium saturated LADH-Cl (Phase I) produces lithium unsaturated LADH-Cl (Phase II) until Al:Li molar ratio 3, which corresponds to an ultimate reversible lithium "adsorption−desorption" capacity of ∼10 mg of Li per g of LADH-Cl. Excessive lithium deintercalation results in the phase structure collapse of LADH-Cl and the formation of gibbsite. The majority of the lithium ions lies in the Al−OH octahedral cavity, regardless of Phase I or II. In Phase II, even the crystal stacking structure is well preserved during LiCl (de)intercalation, and extensive Al-hydroxyl behaved like the intralayer OH as in gibbsite. The Li desolvation and Al−OH reorientation effects are crucial for understanding the relatively high active energy of apparent lithium "adsorption−desorption" behavior in a LADH-Cl sorbent.

ASSOCIATED CONTENT

Supporting Information

The Supporting Information is available free of charge at https://pubs.acs.org/doi/10.1021/acsmaterialsau.3c00063.

Raw materials, experimental setup and procedures, powder XRD characterization and Rietveld refinements, ssNMR characterization, FTIR and Raman characterization, SEM, TEM, and SAED characterization, and DFT and AIMD simulations (PDF)

Atom trajectory generated from AIMD simulations: 1w-I-AIMD for 1w LADH-Cl phase with initial configuration I (MPG)

Atom trajectory generated from AIMD simulations: 1w-II-AIMD for 1w LADH-Cl phase with initial configuration II (MPG)

Atom trajectory generated from AIMD simulations: 1w-III-AIMD for 1w LADH-Cl phase with initial configuration III (MPG)

Atom trajectory generated from AIMD simulations: 2w-I-AIMD for 2w LADH-Cl phase with initial configuration I (MPG)

Atom trajectory generated from AIMD simulations: 2w-II-AIMD for 2w LADH-Cl phase with initial configuration II (MPG)

Atom trajectory generated from AIMD simulations: 2w-III-AIMD for 2w LADH-Cl phase with initial configuration III (MPG)

AUTHOR INFORMATION

Corresponding Author

Dongdong Li − *Qinghai Institute of Salt Lakes, Chinese Academy of Sciences, Xining 810008, P. R. China; Key Lab of Comprehensive and Highly Efficient Utilization of Salt Lake Resources, Chinese Academy of Sciences, Xining 810008, P. R. China;* orcid.org/0000-0002-2206-8298; Phone: +086 13007766878; Email: lidongdong@isl.ac.cn

Authors

Ning Zhang − *College of Science, Central South University of Forestry and Technology, Changsha 410004, P. R. China;* orcid.org/0000-0003-2384-1227

Dandan Gao − *Qinghai Institute of Salt Lakes, Chinese Academy of Sciences, Xining 810008, P. R. China;* orcid.org/0000-0002-3968-4767

Ziyu Zhuang − *Qinghai Institute of Salt Lakes, Chinese Academy of Sciences, Xining 810008, P. R. China*

Dewen Zeng − *Qinghai Institute of Salt Lakes, Chinese Academy of Sciences, Xining 810008, P. R. China; College of Chemistry and Chemical Engineering, Central South University, Changsha 410083, P.R. China;* orcid.org/0000-0003-0858-8606

Complete contact information is available at: https://pubs.acs.org/10.1021/acsmaterialsau.3c00063

Author Contributions

‖D.L. and N.Z. contributed equally to this work.

Notes

The authors declare no competing financial interest.

ACKNOWLEDGMENTS

D.L. thanks the West Light Foundation of Chinese Academy of Sciences (No. 292022000019) and Young Scientist Project of National Key Research and Development Program (No. 2022YFC2906200) for financial support. N.Z. thanks the National Key Research and Development Program (No. 2022YFC3900905), National Natural Science Foundation of China (No. 52234001) and Natural Science Foundation of Hunan Province, China (No. 2023JJ31014) for financial support. We are grateful to Li-Zhi Hong from Shanghai Jiaotong University for ssNMR characterization, Li Han from Qinghai Institute of Salt Lakes, CAS for PXRD characterization (who would like to acknowledge the financial support from The Function Development and Technology Innovation

Project of CAS 2023G104 and 2021 Kunlun Talents Plan of Qinghai Province), and Xiuping Ding from Qinghai Institute of Salt Lakes, CAS for SEM and TEM characterizations. The National Supercomputing Center in Shenzhen is acknowledged for providing the computation resources.

REFERENCES

(1) Kotsupalo, N.; Ryabtsev, A.; Poroshina, I.; Kurakov, A.; Mamylova, E.; Menzheres, L.; Korchagin, M. Effect of Structure on the Sorption Properties of Chlorine-Containing form of Double Aluminum Lithium Hydroxide. *Russ. J. Appl. Chem.* **2013**, *86*, 482−487.

(2) Menzheres, L.; Ryabtsev, A.; Mamylova, E. Synthesis of Selective Sorbent LiCl ·2Al(OH)$_3$· *n* H_2O. *Theor. Found. Chem. Eng.* **2019**, *53*, 821−826.

(3) Warren, P. *Techno-Economic Analysis of Lithium Extraction from Geothermal Brines*; National Renewable Energy Laboratory: Golden, CO, 2021.

(4) Yu, H.; Naidu, G.; Zhang, C.; Wang, C.; Razmjou, A.; Han, D. S.; He, T.; Shon, H. Metal-Based Adsorbents for Lithium Recovery from Aqueous Resources. *Desalination* **2022**, *539*, 115951.

(5) Iyer, R. K.; Kelly, J. C. *Lithium Production from North American Brines*; 2022.

(6) Greim, P.; Solomon, A.; Breyer, C. Assessment of Lithium Criticality in the Global Energy Transition and Addressing Policy Gaps in Transportation. *Nat. Commun.* **2020**, *11*, 4570.

(7) Isupov, V.; Kotsupalo, N.; Nemudry, A.; Menzeres, L. Aluminium Hydroxide as Selective Sorbent of Lithium Salts from Brines and Technical Solutions. *Stud. Surf. Sci. Catal.* **1999**, *120*, 621−652.

(8) Hu, F.; Lin, S.; Li, P.; Yu, J. Quantitative Effects of Desorption Intensity on Structural Stability and Readsorption Performance of Lithium/Aluminum Layered Double Hydroxides in Cyclic Li^+ Extraction from Brines with Ultrahigh Mg/Li Ratio. *Ind. Eng. Chem. Res.* **2020**, *59*, 13539−13548.

(9) Wu, L.; Li, L.; Evans, S. F.; Eskander, T. A.; Moyer, B. A.; Hu, Z.; Antonick, P. J.; Harrison, S.; Paranthaman, M. P.; Riman, R.; et al. Lithium Aluminum-Layered Double Hydroxide Chlorides (LDH): Formation Enthalpies and Energetics for Lithium Ion Capture. *J. Am. Ceram. Soc.* **2019**, *102*, 2398−2404.

(10) Wu, L.; Evans, S. F.; Cheng, Y.; Navrotsky, A.; Moyer, B. A.; Harrison, S.; Paranthaman, M. P. Neutron Spectroscopic and Thermochemical Characterization of Lithium−Aluminum−Layered Double Hydroxide Chloride: Implications for Lithium Recovery. *J. Phys. Chem. C* **2019**, *123*, 20723−20729.

(11) Jayanthi, K.; Neilsen, G.; Rosen, P. F.; Andersen, C. I.; Dickson, M. S.; Evans, S. F.; Paranthaman, M. P.; Woodfield, B. F.; Navrotsky, A. Cryogenic Heat Capacity Measurements and Thermodynamic Analysis of Lithium Aluminum Layered Double Hydroxides (LDHs) with Intercalated Chloride. *Am. Mineral.* **2022**, *107*, 709−715.

(12) Besserguenev, A. V.; Fogg, A. M.; Francis, R. J.; Price, S. J.; O'Hare, D.; Isupov, V. P.; Tolochko, B. P. Synthesis and Structure of the Gibbsite Intercalation Compounds {X = Cl, Br, NO_3} and [$LiAl_2(OH)_6$]Cl ·H_2O using Synchrotron X-ray and Neutron Powder Diffraction. *Chem. Mater.* **1997**, *9*, 241−247.

(13) Hou, X.; Kirkpatrick, R. J. Thermal Evolution of the Cl^--$LiAl_2$ Layered Double Hydroxide: A Multinuclear MAS NMR and XRD Perspective. *Inorg. Chem.* **2001**, *40*, 6397−6404.

(14) Fogg, A. M.; Freij, A. J.; Parkinson, G. M. Synthesis and Anion Exchange Chemistry of Rhombohedral Li/Al Layered Double Hydroxides. *Chem. Mater.* **2002**, *14*, 232−234.

(15) Zhitova, E. S.; Pekov, I. V.; Chaikovskiy, I. I.; Chirkova, E. P.; Yapaskurt, V. O.; Bychkova, Y. V.; Belakovskiy, D. I.; Chukanov, N. V.; Zubkova, N. V.; Krivovichev, S. V.; et al. Dritsite, $Li_2Al_4(OH)_{12}Cl_2{\cdot}3H_2O$, a New Gibbsite-Based Hydrotalcite Supergroup Mineral. *Minerals* **2019**, *9*, 492.

(16) Venkataraman, K.; Pachayappan, L. Synthesis of Nordstrandite and Nordstrandite-Derived Layered Double Hydroxides of Li and Al: A Comparative Study with the Bayerite Counterpart. *Z. Anorg. Allg. Chem.* **2020**, *646*, 1916−1921.

(17) Britto, S.; Kamath, P. V. Structure of Bayerite-Based Lithium-Aluminum Layered Double Hydroxides (LDHs): Observation of Monoclinic Symmetry. *Inorg. Chem.* **2009**, *48*, 11646−11654.

(18) Paranthaman, M. P.; Li, L.; Luo, J.; Hoke, T.; Ucar, H.; Moyer, B. A.; Harrison, S. Recovery of Lithium from Geothermal Brine with Lithium−Aluminum Layered Double Hydroxide Chloride Sorbents. *Environ. Sci. Technol.* **2017**, *51*, 13481−13486.

(19) Menzheres, L.; Kotsupalo, N.; Mamylova, E. Solid-State Interaction of Aluminium Hydroxide with Lithium Salts. *J. Mater. Synth. Process.* **1999**, *7*, 239−244.

(20) Fogg, A. M.; Dunn, J. S.; Shyu, S.-G.; Cary, D. R.; O'Hare, D. Selective Ion-Exchange Intercalation of Isomeric Dicarboxylate Anions into the Layered Double Hydroxide [$LiAl_2(OH)_6$]Cl ·H_2O. *Chem. Mater.* **1998**, *10*, 351−355.

(21) Thomas, G. S.; Kamath, P. V.; Kannan, S. Variable Temperature PXRD Studies of $LiAl_2(OH)_6X$ ·H_2O (X= Cl, Br): Observation of Disorder-Order Transformation in the Interlayer. *J. Phys. Chem. C* **2007**, *111*, 18980−18984.

(22) Wimpenny, J.; Colla, C. A.; Yu, P.; Yin, Q.-Z.; Rustad, J. R.; Casey, W. H. Lithium Isotope Fractionation during Uptake by Gibbsite. *Geochim. Cosmochim. Acta* **2015**, *168*, 133−150.

(23) Nagendran, S.; Kamath, P. V. Synthon Approach to Structure Models for the Bayerite-Derived Layered Double Hydroxides of Li and Al. *Inorg. Chem.* **2017**, *56*, 5026−5033.

(24) Rodríguez-Carvajal, J. Recent Advances in Magnetic Structure Determination by Neutron Powder Diffraction. *Physica B Condens. Matter* **1993**, *192*, 55−69.

(25) Massiot, D.; Fayon, F.; Capron, M.; King, I.; Le Calvé, S.; Alonso, B.; Durand, J.-O.; Bujoli, B.; Gan, Z.; Hoatson, G. Modelling One and Two-dimensional Solid-State NMR Spectra. *Magn. Reson. Chem.* **2002**, *40*, 70−76.

(26) Schreinemakers, F. Graphische Ableitungen aus den lösungs-Isothermen Eines Doppelsalzes und Seiner Komponenten und Mögliche formen der Umwandlungskurve. *Z. Phys. Chem.* **1893**, *11*, 75−109.

(27) Purdon, F. F.; Slater, V. W. *Aqueous Solution and the Phase Diagram*; E. Arnold & Company: London, 1946; pp 63−64.

(28) Fogg, A. M.; O'Hare, D. Study of the Intercalation of Lithium Salt in Gibbsite using Time-Resolved in Situ X-ray Diffraction. *Chem. Mater.* **1999**, *11*, 1771−1775.

(29) Vyalikh, A.; Zesewitz, K.; Scheler, U. Hydrogen Bonds and Local Symmetry in the Crystal Structure of Gibbsite. *Magn. Reson. Chem.* **2010**, *48*, 877−881.

(30) Ruan, H.; Frost, R.; Kloprogge, J. T. Comparison of Raman Spectra in Characterizing Gibbsite, Bayerite, Diaspore and Boehmite. *J. Raman. Spectrosc.* **2001**, *32*, 745−750.

https://doi.org/10.1021/acsmaterialsau.3c00063
ACS Mater. Au 2024, 4, 45−54